Eur. Phys. J. C 17, 473–486 (2000)
Digital Object Identifier (DOI) 10.1007/s100520000480

THE EUROPEAN
PHYSICAL JOURNAL C


# Possible enhancement of the $e^+e^- \to H^\pm W^\mp$ cross section in the two-Higgs-doublet model

S. Kanemura[a]

Institut für Theoretische Physik der Universität Karlsruhe, 76128 Karlsruhe, Germany

Received: 26 November 1999 / Revised version: 7 July 2000 /
Published online: 8 September 2000 – © Springer-Verlag 2000

**Abstract.** The production process of the charged Higgs boson associated with a $W$ boson at electron–positron colliders is discussed in the two-Higgs-doublet model (2HDM) and in the minimal supersymmetric standard model (MSSM). The process is induced at one-loop level in these models. We examine how much the cross section can be enhanced by quark- and Higgs-loop effects. In the non-SUSY 2HDM, in addition to large top–bottom ($t$–$b$) loop effects for small $\tan\beta$ ($\ll (m_t/m_b)^{1/2}$), the Higgs-loop diagrams can contribute to the cross section to some extent for moderate $\tan\beta$ values. For larger $\tan\beta$ ($\gg (m_t/m_b)^{1/2}$), such an enhancement by the Higgs non-decoupling effects is bounded by the requirement of the validity of perturbation theory. In the MSSM with heavy superpartner particles, only the $t$–$b$ loops enhance the cross section while Higgs-loop effects are very small.

## 1 Introduction

The Higgs sector has not yet been confirmed experimentally. In the near future a neutral Higgs boson may be discovered at Tevatron II or LHC, by which the standard picture of particle physics may be completed. The exploration of additional Higgs bosons will then be very important in order to confirm the extended Higgs sectors from the minimal Higgs sector in the standard model (SM). Actually various theoretical insights suggest such extensions: supersymmetry (SUSY), extra $CP$-violating phases, a source of neutrino masses, a remedy for the strong $CP$ problem and so on. Most of the extended Higgs models include charged and $CP$-odd Higgs bosons. Therefore the discovery of a charged Higgs boson, $H^\pm$, or a $CP$-odd Higgs boson, $A^0$, will confirm the extended versions of the Higgs sector directly. At LHC, the search of these extra Higgs bosons is also one of the most important tasks. In addition, measurements with considerable precision of high-energy phenomena may be possible at future linear colliders (LCs) such as JLC, NLC and TESLA [1].

In this paper, we discuss the charged-Higgs boson production process associated with a $W$ boson at LCs, $e^+e^- \to H^\pm W^\mp$, in the two-Higgs-doublet model (2HDM) including the minimal supersymmetric standard model (MSSM) with superheavy superpartner particles. By neglecting the electron mass the process disappears at tree level because there are no tree $H^\pm W^\mp V$ couplings ($V = \gamma$ and $Z^0$) in these models. Since these couplings occur at the one-loop level [2–4], the process $e^+e^- \to H^\pm W^\mp$ is induced at this level. At LCs, one of the main processes for the charged-Higgs search is the $H^\pm$-pair production [5], whose cross section may be large enough to be detected if $H^\pm$ is much lighter than the threshold, $s^{1/2}/2$. The process rapidly decreases for heavier $H^\pm$ even if the mass is below the threshold. In this case $e^+e^- \to H^\pm W^\mp$ becomes important as a complementary process if its cross section can be large enough to be detected. Our question here is how much this loop-induced process can grow in the non-SUSY 2HDM as well as in the MSSM.

The magnitude of the cross section for $e^+e^- \to H^\pm W^\mp$ directly shows the dynamics of particles in the loop because there is no tree-level contribution. We here consider one-loop contributions of quarks, gauge bosons and Higgs bosons.

In particular, the top–bottom ($t$–$b$) loop effects are expected to be sizable, because the Yukawa-coupling constants are proportional to the quark masses so that the decoupling theorem by Appelquist and Carazzone [6] is not applicable to this case. The naive power-counting argument shows that quadratic quark-mass terms appear in the amplitude with a longitudinally polarized $W$ boson. Therefore the $t$–$b$ loops can greatly contribute to the cross section depending on $\tan\beta$.

In the non-SUSY 2HDM, the Higgs-loop contributions can also be large when the Higgs self-coupling constants are proportional to the Higgs boson masses. The effects of the heavy Higgs bosons in the loop then do not decouple in the large mass limit. Instead, the quadratic mass terms of these Higgs bosons can appear in the amplitude [4,7,8], so that larger Higgs-loop effects are expected for heavier Higgs bosons in the loop. By contrast, if the masses of the extra Higgs bosons are determined mainly by the indepen-

[a] e-mail: kanemu@particle.physik.uni-karlsruhe.de

dent scale of the vacuum expectation value ($\sim 246\,\mathrm{GeV}$), the Higgs-loop contributions tend to decouple for large extra-Higgs boson masses. The MSSM Higgs sector corresponds to this case, so its loop effects cannot be very large.

The main purpose of this paper is to confirm the above discussion analytically and numerically and to see the possible enhancement of the cross section by these non-decoupling effects under the requirement of the validity of perturbation theory [9–11, 7]. The information from available experimental data such as the $\rho$ parameter constraint [12] and the $b \to s\gamma$ results [13, 14] are also taken into account.

We find that the cross section can be quite large for small $\tan\beta$ ($\ll (m_t/m_b)^{1/2}$) because of the $t$–$b$ loop effects. In addition, in the non-SUSY 2HDM, the cross section can grow to some extent by the Higgs non-decoupling effects for moderate values of $\tan\beta$. For larger $\tan\beta$ ($\gg (m_t/m_b)^{1/2}$) such an enhancement by the Higgs-loop effects is strongly bounded by the condition for the perturbation, and the cross section becomes smaller.

In Sect. 2, the 2HDM is reviewed briefly to fix our notation. The calculation of the cross section is explained in Sect. 3. After some analytic discussion of the amplitude in Sect. 4, we present our numerical results in Sect. 5. The conclusions are given in Sect. 6. Details of the analytic results of the calculation are shown in the Appendix.

## 2 The 2HDM

The 2HDM with a softly broken discrete symmetry under the transformation $\Phi_1 \to \Phi_1$, $\Phi_2 \to -\Phi_2$ is assumed. The Higgs sector is given by

$$\begin{aligned}\mathcal{L}_{\mathrm{THDM}}^{\mathrm{int}} &= \mu_1^2 \left|\Phi_1\right|^2 + \mu_2^2 \left|\Phi_2\right|^2 + \left\{\mu_3^2 \left(\Phi_1^\dagger \Phi_2\right) + \mathrm{h.c.}\right\} \\ &\quad - \lambda_1 \left|\Phi_1\right|^4 - \lambda_2 \left|\Phi_2\right|^4 - \lambda_3 \left|\Phi_1\right|^2 \left|\Phi_2\right|^2 \\ &\quad - \lambda_4 \left(\mathrm{Re}\Phi_1^\dagger \Phi_2\right)^2 - \lambda_5 \left(\mathrm{Im}\Phi_1^\dagger \Phi_2\right)^2 . \end{aligned} \tag{1}$$

This potential includes the MSSM Higgs sector as a special case. We here neglect all the $CP$-violating phases just for simplicity, and all the coupling constants and masses are then real in (1). From the doublets $\Phi_1$ and $\Phi_2$ ($\langle\Phi_i\rangle \equiv v_i/2^{1/2}$ and $(v_1^2+v_2^2)^{1/2} \sim 246\,\mathrm{GeV}$), five massive eigenstates as well as three Nambu–Goldstone modes ($w^\pm$ and $z^0$) are obtained; that is, two $CP$-even neutral bosons $h^0$ and $H^0$ diagonalized by the mixing angle $\alpha$, one pair of charged Higgs bosons $H^\pm$, and one $CP$-odd neutral Higgs boson $A^0$, where $h^0$ is lighter than $H^0$. In addition to the four mass parameters $m_{h^0}$, $m_{H^0}$, $m_{H^\pm}$ and $m_{A^0}$, we have two mixing angles $\alpha$ and $\beta$ ($\tan\beta = v_2/v_1$) and one free dimension-full parameter $M$ corresponding to the soft-breaking mass ($M^2 \equiv \mu_3^2/(\sin\beta\cos\beta)$).

Tree-level relations among the coupling constants and the masses are then given by [4]

$$\lambda_1 = \frac{1}{2v^2\cos^2\beta}(\cos^2\alpha m_{H^0}^2 + \sin^2\alpha m_{h^0}^2 - \sin^2\beta M^2), \tag{2}$$

$$\lambda_2 = \frac{1}{2v^2\sin^2\beta}(\sin^2\alpha m_{H^0}^2 + \cos^2\alpha m_{h^0}^2 - \cos^2\beta M^2), \tag{3}$$

$$\lambda_3 = \frac{\sin 2\alpha}{v^2\sin 2\beta}(m_{H^0}^2 - m_{h^0}^2) + \frac{2m_{H^\pm}^2}{v^2} - \frac{1}{v^2}M^2, \tag{4}$$

$$\lambda_4 = -\frac{2m_{H^\pm}^2}{v^2} + \frac{2}{v^2}M^2, \tag{5}$$

$$\lambda_5 = \frac{2}{v^2}(m_{A^0}^2 - m_{H^\pm}^2). \tag{6}$$

As for the Yukawa interaction, two kinds of couplings are possible in our model: we call them Model I and Model II in accordance with [15]. The Yukawa interaction with respect to the charged-Higgs boson is expressed by

$$\begin{aligned}\mathcal{L}_{Htb} &= \overline{b}\left\{\frac{y_b}{2}\tan\beta(1-\gamma_5) + \frac{y_t}{2}\cot\beta(1+\gamma_5)\right\} tH^- \\ &\quad + \mathrm{h.c.},\end{aligned} \tag{7}$$

where

$$y_b = \frac{\sqrt{2}m_b}{v}\cot\beta, \qquad y_t = \frac{\sqrt{2}m_t}{v}\cot\beta \quad (\mathrm{ModelI}), \tag{8}$$

or

$$y_b = \frac{\sqrt{2}m_b}{v}\tan\beta, \qquad y_t = \frac{\sqrt{2}m_t}{v}\cot\beta \quad (\mathrm{ModelII}). \tag{9}$$

Here Model II corresponds to the MSSM Yukawa interaction.

## 3 The calculation for $e^+e^- \to H^-W^+$

We consider the process $e^-(\tau, k) + e^+(-\tau, \overline{k}) \to H^-(p) + W^+(\overline{p}, \overline{\lambda})$, where $\tau = \pm 1$ and $\overline{\lambda} = 0, \pm 1$ are the helicities of the electron and the $W^+$ boson; $k$ and $\overline{k}$ are the incoming momenta of the electron and the positron, while $p$ and $\overline{p}$ are the outgoing momenta of $H^-$ and $W^+$, respectively. The helicity amplitude may be written

$$\mathcal{M}(k, \overline{k}, \tau; p, \overline{p}, \overline{\lambda}) = \sum_{i=1}^{3} F_{i,\tau}(s,t) K_{i,\tau}(k, \overline{k}, \tau; p, \overline{p}, \overline{\lambda}), \tag{10}$$

where the form factors $F_{i,\tau}(s,t)$ include all the dynamics that depends on the model. The kinematical factors are expressed by

$$K_{i,\tau}(k, \overline{k}, \tau; p, \overline{p}, \overline{\lambda}) = j_\mu(k, \overline{k}, \tau) T_i^{\mu\beta} \epsilon_\beta(\overline{p}, \overline{\lambda})^*, \tag{11}$$

where $j_\mu(k, \overline{k}, \tau)$ is the electron current and $\epsilon_\beta(\overline{p}, \overline{\lambda})^*$ is the polarization vector of the $W$ boson. The basis tensors $T_i^{\mu\beta}$ are defined by

$$T_1^{\mu\beta} = g^{\mu\beta}, \tag{12}$$

$$T_2^{\mu\beta} = \frac{1}{m_W^2} P^\mu P^\beta, \tag{13}$$

$$T_3^{\mu\beta} = \frac{\mathrm{i}}{m_W^2} \epsilon^{\mu\beta\rho\sigma} P_\rho q_\sigma, \tag{14}$$

**Table 1.** The list of the kinematical factors $K_{i,\tau}(k,\overline{k},\overline{\lambda})$

| | $K_{1,\tau}(k,\overline{k},\overline{\lambda})$ | $K_{2,\tau}(k,\overline{k},\overline{\lambda})$ | $K_{3,\tau}(k,\overline{k},\overline{\lambda})$ |
|---|---|---|---|
| $\overline{\lambda}=0$ | $-1/(2m_W)(s-m_{H^\pm}^2+m_W^2)\sin\Theta$ | $1/2\frac{s^2}{m_W^3}\beta_{HW}^2\sin\Theta$ | $0$ |
| $\overline{\lambda}=\pm$ | $(s/2)^{1/2}(\mp\cos\Theta+\tau)$ | $0$ | $-s/m_W^2(\frac{s}{2})^{1/2}\beta_{HW}(\cos\Theta\mp\tau)$ |

where $P^\mu \equiv p^\mu - \overline{p}^\mu$, $q^\mu \equiv p^\mu + \overline{p}^\mu = k^\mu + \overline{k}^\mu$ and $\epsilon^{0123} = -1$. In Table 1, the explicit expressions for each $K_{i,\tau}$ in the center-of-mass frame are listed by using $\beta_{HW}$ and the scattering angle $\Theta$:

$$\beta_{HW} = \sqrt{1 - \frac{2(m_W^2+m_{H^\pm}^2)}{s} + \frac{(m_W^2-m_{H^\pm}^2)^2}{s^2}}, \quad (15)$$

$$\cos\Theta = \frac{2t+s-m_{H^\pm}^2-m_W^2}{s\beta_{HW}}, \quad (16)$$

where $s$ and $t$ are the Mandelstam variables ($s = (k+\overline{k})^2 = (p+\overline{p})^2$, $t = (k-p)^2 = (\overline{k}-\overline{p})^2$). The total cross section is calculated according to the formula

$$\sigma(s) = \frac{1}{16\pi}\frac{1}{s^2} \times \int_{t_{\min}}^{t_{\max}} \frac{1}{2}\sum_\tau\sum_{\overline{\lambda}} \left|\mathcal{M}(k,\overline{k},\tau;p,\overline{p},\overline{\lambda})\right|^2 \mathrm{d}t, \quad (17)$$

where $t_{\max}$ and $t_{\min}$ are defined by

$$t_{\max} = \frac{1}{2}(m_{H^\pm}^2 + m_W^2 - s + s\beta_{HW}), \quad (18)$$

$$t_{\min} = \frac{1}{2}(m_{H^\pm}^2 + m_W^2 - s - s\beta_{HW}). \quad (19)$$

Our formalism here is consistent with that for $e^-e^+ \to \chi^-W^+$ ($\chi^-$ is for the charged Goldstone boson) in [16] in the limit $m_{H^\pm}^2 \to m_\chi^2$ and also with that for $e^-e^+ \to H^0\gamma$ in [17].

In the calculation, the form factors $F_{i,\tau}(s,t)$ may be decomposed according to each type of Feynman diagram (Fig. 1) as

$$F_{i,\tau}(s,t) = F_{i,\tau}^\gamma(s) + F_{i,\tau}^Z(s) + F_{i,\tau}^t(t) + F_{i,\tau}^{\mathrm{box}}(s,t) + \delta F_{i,\tau}(s,t), \quad (20)$$

where $F_{i,\tau}^V$ ($V=\gamma$ and $Z$) are the contributions from the one-loop-induced $HWV$ vertices (Fig. 1a). These $HWV$ vertices are defined as $\mathrm{i}gm_W V_{\mu\nu}^{HWV}$ (Fig. 2), in which $V_{\mu\nu}$ may be expressed by [2,4]

$$\begin{aligned} V_{\mu\nu}^{HWV}&(m_{H^\pm}^2,p_W^2,p_V^2) \\ &= F^{HWV}(m_{H^\pm}^2,p_W^2,p_V^2)g_{\mu\nu} \\ &+G^{HWV}(m_{H^\pm}^2,p_W^2,p_V^2)\frac{p_{V\mu}p_{W\nu}}{m_W^2} \\ &+\mathrm{i}H^{HWV}(m_{H^\pm}^2,p_W^2,p_V^2)\frac{p_V^\rho p_W^\sigma}{m_W^2}\epsilon_{\mu\nu\rho\sigma}, \end{aligned} \quad (21)$$

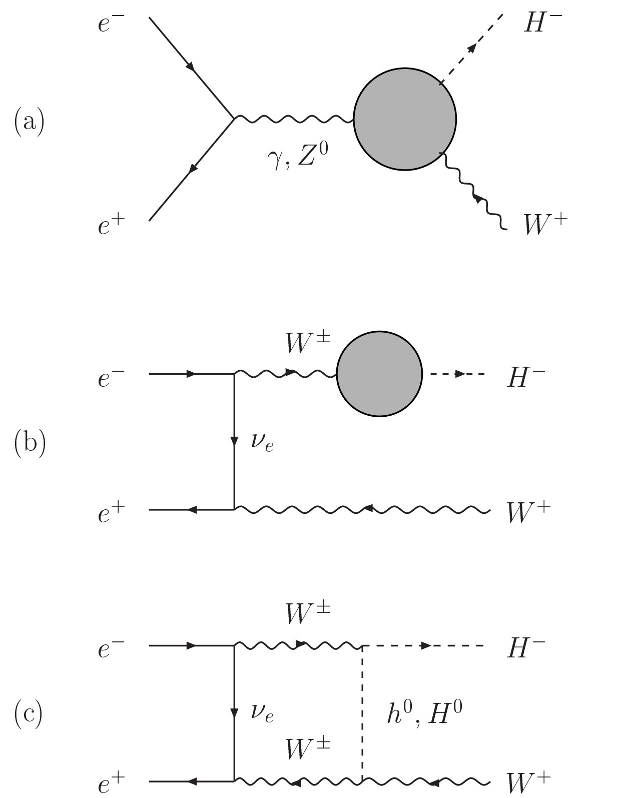


**Fig. 1a–c.** The diagrams for $e^+e^- \to H^-W^+$. The circles in **a** and **b** represent all one-loop diagrams relevant to the $HWV$ vertices ($V=\gamma, Z^0$) and the $HW$ mixing. The arrows on the $H^\pm$ bosons and the $W$ boson lines indicate the flow of negative electric charge

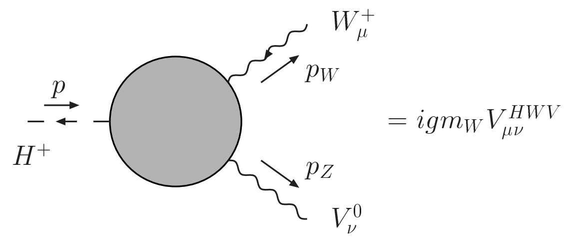


**Fig. 2.** The $HWV$ vertices ($V=\gamma, Z^0$). The arrows on the $H^\pm$ boson and the $W$ boson lines indicate the flow of negative electric charge

where $p_H$ is the incoming momentum of $H^-$, and $p_V$ ($V = Z$ or $\gamma$) and $p_W$ are the outgoing momenta of the $V$ and $W$ bosons, respectively. The form factors $F_{i,\tau}^V(s)$ are then expressed by

$$F_{1,\tau}^V(s) = gm_W C_V \frac{1}{s-m_V^2} F^{HWV}(m_W^2, s, m_{H^\pm}^2), \quad (22)$$

$$F_{2,\tau}^V(s) = g m_W C_V \frac{1}{s-m_V^2}\frac{1}{2} G^{HWV}(m_W^2, s, m_{H^\pm}^2), \quad (23)$$

$$F_{3,\tau}^V(s) = g m_W C_V \frac{1}{s-m_V^2}\frac{-1}{2} H^{HWV}(m_W^2, s, m_{H^\pm}^2), \quad (24)$$

where $m_V$ is mass of the neutral gauge bosons ($m_Z$ and $m_\gamma(=0)$), and $C_V$ are defined by $C_\gamma = eQ_e$ and $C_Z = g_Z(T_e^3 - s_W^2 Q_e)$ ($e = g s_W = g_Z s_W c_W$), where $Q_e = -1$, and $T_e^3 = -1/2$ (0) for the electron with helicity $\tau = -1$ (+1). The explicit formulas of $F^{HWV}$, $G^{HWV}$, $H^{HWV}$ are given in Appendix A.1. $F_{i,\tau}^t(s,t)$ is the contribution of the $t$ channel diagram with the one-loop $H^-W^+$ mixing diagrams (Fig. 1b) and the box-diagram contributions are expressed by $F_{i,\tau}^{\rm box}$ (Fig. 1c). We also show the explicit results for $F_{i,\tau}^t$ and $F_{i,\tau}^{\rm box}$ in Appendix A.3 and A.4, respectively. Each one-loop-diagram contribution to $F_1(s,t)$ except for $F_{1,\tau}^{\rm box}$ includes an ultraviolet divergence. After summing up the contributions $F_{i,t}^V$, $F_{i,\tau}^t$, and $F_{i,\tau}^{\rm box}$, the divergence is canceled out because there is no tree-level contribution.

Although the amplitude is finite already, by making the renormalization for the $WH$ and $wH$ two-point functions a finite counterterm, $\delta F_{i,\tau}$, is introduced to this process [18,19][1]. By rewriting the fields $w^\pm$ and $H^\pm$ on shifting $\beta \to \beta - \delta\beta$ as

$$\begin{pmatrix} w^\pm \\ H^\pm \end{pmatrix} \to \begin{pmatrix} Z_{w^\pm}^{1/2} & Z_{wH}^{1/2} \\ Z_{Hw}^{1/2} & Z_{H^\pm}^{1/2} \end{pmatrix} \begin{pmatrix} 1 & -\delta\beta \\ \delta\beta & 1 \end{pmatrix} \begin{pmatrix} w^\pm \\ H^\pm \end{pmatrix}$$
$$\equiv \begin{pmatrix} 1+\frac{1}{2}Z_{w^\pm}^{(1)} & a_{wH}^{(1)} \\ a_{Hw}^{(1)} & 1+\frac{1}{2}Z_{H^\pm}^{(1)} \end{pmatrix} \begin{pmatrix} w^\pm \\ H^\pm \end{pmatrix}; \quad (25)$$

the relevant counterterms are extracted from the kinematic terms of the Higgs sector as follows:

$$\mathcal{L}^{\rm count.} = {\rm i} a_{wH}^{(1)} \frac{gv}{2} W_\mu^- \partial^\mu H^+ - a_{wH}^{(1)} \frac{g^2 v}{2}\frac{s_W^2}{c_W} W_\mu Z^\mu H^+ + a_{wH}^{(1)} \frac{g^2 v}{2} s_W W_\mu \gamma^\mu H^+ + {\rm h.c.} \quad (26)$$

For the $WH$ mixing we take the renormalization condition

$$\mathrm{Re}\left(\Pi_{WH}^{\rm reno.}(m_{H^\pm}^2)\right) = \mathrm{Re}\left(\Pi_{WH}(m_{H^\pm}^2)\right) + \Pi_{WH}^{\rm count.} = 0, \quad (27)$$

where $\Pi_{WH}(p^2)$ is given in (61) in the Appendix. We then obtain

$$a_{wH}^{(1)} = \frac{1}{m_W}\mathrm{Re}\left(\Pi_{WH}(m_{H^\pm}^2)\right), \quad (28)$$

so that the counterterms not only for $WH$ mixing but also for the $HWV$ vertices are obtained by using (26). Next, (25) also produces the $wH$ mixing ($w$ is for the charged Goldstone boson). We fix the counterterm so as to satisfy the renormalization condition [19]

$$\mathrm{Re}\left(\Pi_{Hw}^{\rm reno.}(m_{H^\pm}^2)\right) = \mathrm{Re}\left(\Pi_{Hw}(m_{H^\pm}^2)\right) + \Pi_{Hw}^{\rm count.} = 0. \quad (29)$$

[1] See also Note added in proof

The finite counterterms for the form factors, $\delta F_{i,\tau}$ in (20), are then obtained as we show in Appendix A.5.

## 4 Non-decoupling mass effects

Here we present an analytic discussion of the amplitudes to find the cases in which the cross section becomes large for a given $s^{1/2}$ in the non-SUSY 2HDM.

Let us consider the quark-loop contributions to the amplitudes first. They do not decouple in the heavy-quark limit because the decoupling theorem [6] does not work for the Yukawa interactions in which the couplings are proportional to the squared masses. Hence larger one-loop effects take place for heavier quark masses[2]. In the helicity amplitude with a longitudinally polarized $W$ boson, powerlike top- or bottom-quark mass contributions appear via the factor of $m_t^2 \cot\beta$ or $m_b^2 \tan\beta$ in Model II. The linear appearance of $\cot\beta$ or $\tan\beta$ in each factor comes from the fact that one $tbH^\pm$ Yukawa coupling is included in each $t$–$b$ loop diagram[3]. Each factor becomes large for small $\tan\beta$ ($\ll (m_t/m_b)^{1/2}$) or for large $\tan\beta$ ($\gg (m_t/m_b)^{1/2}$), respectively. In our analysis, we take into account theoretical lower and upper bounds of $\tan\beta$ taking as a criterion for the upper limit of the top-Yukawa coupling $y_t$ ($\propto m_t/\sin\beta$) and the bottom-Yukawa coupling $y_b$ ($\propto m_b/\cos\beta$) the requirement of the validity of perturbation theory. Under the same criterion for both the top- and bottom-Yukawa coupling constants, the factor $m_t^2 \cot\beta$ at the lowest $\tan\beta$ value is by $m_t/m_b$ greater than the factor $m_b^2 \tan\beta$ at the highest $\tan\beta$ value. Therefore, the helicity amplitude becomes large especially for small $\tan\beta$ ($\ll (m_t/m_b)^{1/2}$) by the $t$–$b$ loop contributions[4]. In Model I, $\tan\beta$ is just replaced by $\cot\beta$ in the coefficient above, hence this change does not affect the above discussion. Therefore in both Model I and II, we expect to have sizable cross sections for small $\tan\beta$ values.

Next we discuss the Higgs-loop contributions. The non-decoupling effects of the heavy Higgs bosons appear only when the Higgs sector has a special property: the Higgs masses squared are expressed like $\sim \lambda_i v^2$, where $\lambda_i$ is a combination of the Higgs self-coupling constants. This corresponds to $M \ll v$ in our notation [4,7], where $M$ is the scale of the soft breaking of the discrete symmetry. In this case, similarly to the Yukawa interaction, the terms of $\mathcal{O}(m_{H_i^0}^2/v^2)$ appear in the helicity amplitude with a longitudinally polarized $W$ boson, where $H_i^0$ represent heavy neutral Higgs bosons in the loop. Therefore, in the non-SUSY 2HDM with small soft-breaking mass $M$, these mass effects of the heavy Higgs bosons may enhance the

[2] We here call them the non-decoupling effects

[3] The $tbH^-$ coupling gives $m_t \cot\beta$ and $m_b \tan\beta$, and the other $m_t$ and $m_b$ comes from the $tbW_{\rm L}^+$ coupling ($W_{\rm L}$ represents the longitudinal $W$ boson). By the chirality argument other combinations such as $m_t m_b \cot\beta$ and $m_t m_b \cot\beta$ disappear

[4] Similar top–bottom-quark effects are observed in the cross section of $e^+e^- \to A^0 V$ ($V = \gamma, Z^0$) [20]

amplitude in addition to the $t$–$b$ loop effects. Clearly, this situation is quite different from the MSSM-like Higgs sector, where large masses of the extra Higgs bosons are possible only by taking a large $M$ ($\gg \lambda_i v^2 = \mathcal{O}(g^2v^2)$)[5].

In order to see the leading non-decoupling effects (the quadratic-mass terms in the large mass limit for particles in the loop) analytically, let us consider the amplitude with a longitudinally polarized $W$ boson in a limiting case. They are extracted from the full expression of the amplitude by taking the masses of $h^0$, $H^0$ and $A^0$ much larger than $m_W$ and $m_{H^\pm}$ setting $M = 0$[6];

$$\begin{aligned}
&\mathcal{M}(k,\overline{k},\tau;p,\overline{p},\overline{\lambda}=0)\\
&= \sin\Theta \frac{g^2}{c_W^2}\frac{T_e^3}{16\pi^2v^2}\left[\frac{3}{2}\left\{\frac{m_{H^0}^2 m_{A^0}^2}{m_{H^0}^2-m_{A^0}^2}\ln\frac{m_{H^0}^2}{m_{A^0}^2}\right.\right.\\
&\left. -\frac{m_{h^0}^2 m_{A^0}^2}{m_{h^0}^2-m_{A^0}^2}\ln\frac{m_{h^0}^2}{m_{A^0}^2}\right\} J(\alpha,\beta) - \left\{\frac{c_{2W}}{2}m_{H^0}^2 + \frac{3}{4}\right.\\
&\left.\times \frac{m_{H^0}^2 m_{A^0}^2}{m_{H^0}^2-m_{A^0}^2}\ln\frac{m_{H^0}^2}{m_{A^0}^2}\right\} K(\alpha,\beta) - \left\{\frac{c_{2W}}{2}m_{h^0}^2 + \frac{3}{4}\right.\\
&\left.\left.\times \frac{m_{h^0}^2 m_{A^0}^2}{m_{h^0}^2-m_{A^0}^2}\ln\frac{m_{h^0}^2}{m_{A^0}^2}\right\} L(\alpha,\beta) - \frac{N_c}{2}m_t^2\cot\beta\right]\\
&+\sin\Theta\frac{g^2 s_W^2 Q_e}{16\pi^2v^2}\left[\frac{3}{2}\left\{\frac{m_{H^0}^2 m_{A^0}^2}{m_{H^0}^2-m_{A^0}^2}\ln\frac{m_{H^0}^2}{m_{A^0}^2} - \frac{m_{h^0}^2 m_{A^0}^2}{m_{h^0}^2-m_{A^0}^2}\right.\right.\\
&\left.\times\ln\frac{m_{h^0}^2}{m_{A^0}^2}\right\} J(\alpha,\beta) - \left\{\frac{1}{2c_W^2}m_{H^0}^2 - \frac{3}{4}\frac{m_{H^0}^2 m_{A^0}^2}{m_{H^0}^2-m_{A^0}^2}\right.\\
&\left.\ln\frac{m_{H^0}^2}{m_{A^0}^2}\right\} K(\alpha,\beta) - \left\{\frac{1}{2c_W^2}m_{h^0}^2 - \frac{3}{4}\frac{m_{h^0}^2 m_{A^0}^2}{m_{h^0}^2-m_{A^0}^2}\right.\\
&\left.\left.\times\ln\frac{m_{h^0}^2}{m_{A^0}^2}\right\} L(\alpha,\beta) + \frac{N_c}{2c_W^2}m_t^2\cot\beta\right] + \mathcal{O}\left(\frac{s}{m_{H_i^0}^2}\right), \quad (30)
\end{aligned}$$

where $H_i^0$ represents $h^0$, $H^0$ and $A^0$, and

$$J(\alpha,\beta) = \sin(\alpha-\beta)\cos(\alpha-\beta), \quad (31)$$

$$K(\alpha,\beta) = \sin^2\alpha\cot\beta - \cos^2\alpha\tan\beta, \quad (32)$$

$$L(\alpha,\beta) = \cos^2\alpha\cot\beta - \sin^2\alpha\tan\beta. \quad (33)$$

From the expression (30), we expect that the amplitude can become large by the non-decoupling effects of the heavy Higgs bosons as well as those of the top quark. The Higgs effects grow for large or small $\tan\beta$: see (31)–(33).

The non-SUSY 2HDM receives rather strong theoretical constraints. First from the requirement of the validity of perturbation theory, all the Higgs self-coupling and Yukawa coupling constants should not be very large [9–11]. We here set a rather conservative criterion corresponding to [7]; that is, for the Yukawa couplings

$$y_b^2, y_t^2 < 4\pi, \quad (34)$$

and for the Higgs self-coupling constants

$$|\lambda_1|, |\lambda_2|, |\lambda_3|, \frac{1}{4}|\lambda_4 \pm \lambda_5| < 4\pi. \quad (35)$$

[5] In the MSSM, $m_A$ corresponds to $M$

[6] This expression is for the $\delta F_{i,\tau} = 0$ case

These conditions give constraints on the relations among the masses, mixing angles and the soft-breaking mass. For example, from the condition for $\lambda_1$, we obtain by using (2)

$$(m_{H^0}^2 - M^2)\tan^2\beta \lesssim 8\pi v^2, \quad (36)$$

for the case of $\alpha = \beta - \pi/2$ and $m_{H^0}^2 \gg m_{h^0}^2$. This means that it is difficult to take a large $m_{H^0}$ and a large $\tan\beta$ simultaneously with $M^2 \sim 0$. We include all these constraints in our numerical analysis.

Finally, the 2HDM is constrained from the experimental precision data [12], especially those for the $\rho$ parameter: the additional contribution of the 2HDM Higgs sector should be small. We here employ the same condition as in [7]; $\Delta\rho_{\text{2HDM}} = -0.0020 - 0.00049(m_t - 175\,\text{GeV})/(5\,\text{GeV})$ $\pm 0.0027$. In order to satisfy this there are mainly two kinds of possibilities for the parameter choice.

(A) The Higgs sector is custodial $SU(2)_V$ symmetric ($m_{H^\pm}^2 \sim m_{A^0}^2$).
(B) The Higgs sector is not custodial $SU(2)_V$ symmetric, but there are some relations among the parameters to keep a small $\Delta\rho_{\text{2HDM}}$: $m_{H^\pm}^2 \sim m_{H^0}^2$ or $m_{H^\pm}^2 \sim m_{h^0}^2$ with $\alpha \sim \beta - \pi/2$ or $\alpha \sim \beta$, respectively [15]. Also, a recent study for the $b \to s\gamma$ results [13] gives a constraint on the charged Higgs boson mass ($m_{H^\pm} \gtrsim 160\,\text{GeV}$) [14].

By taking into account all the theoretical and experimental constraints above, the best choice for the maximal Higgs contributions to the cross section is to take the case (B) and then to choose $m_{A^0}$ and $\tan\beta$ as large as possible under the conditions (34) and (35).

## 5 Numerical evaluation

We here show our numerical results. According to the above analytic discussion, the seven free parameters of the Higgs sector in the non-SUSY 2HDM ($m_{h^0}^2$, $m_{H^0}^2$, $m_{H^\pm}^2$, $m_{A^0}^2$, $\alpha$, $\beta$ and $M$) are chosen in the following way.

To obtain larger Higgs contributions, we take the choice (B) of the previous section. Since $m_{h^0} < m_{H^0}$, it is better to set $\alpha = \beta - \pi/2$ (or $\alpha = 0$) for a larger cross section for $\tan\beta > 1$ ($K(\alpha,\beta) > 1$) (see (32)). If we choose $\alpha = \beta$ (or $\alpha = \pi/2$), then such an enhancement takes place for small $\tan\beta$ ($L(\alpha,\beta) \sim 1$). Any other choice of $\alpha$ leads to smaller cross sections. As for the quark loops, although we here adopt Model II for the Yukawa couplings in the actual calculation in the 2HDM, it is clear that there is no difference between Model I and II for the cross section except for the large $\tan\beta$ regime. If we assume the MSSM Higgs sector, there are two free parameters: $m_{H^\pm}$ and $\tan\beta$, and all the other parameters are related to these two parameters [15]. As for the quark masses we here fix these as $m_t = 175\,\text{GeV}$ and $m_b = 5\,\text{GeV}$.

To begin with, we show the total cross section for $m_{H^\pm} = 200\,\text{GeV}$ at $s^{1/2} = 500\,\text{GeV}$ as a function of $\tan\beta$ (Fig. 3). The region of $\tan\beta$ is $0.28 < \tan\beta < 123$ taking into account the condition (34)[7], while we switch off

[7] As for the constraint for $\tan\beta$ in the MSSM, see [21–23]

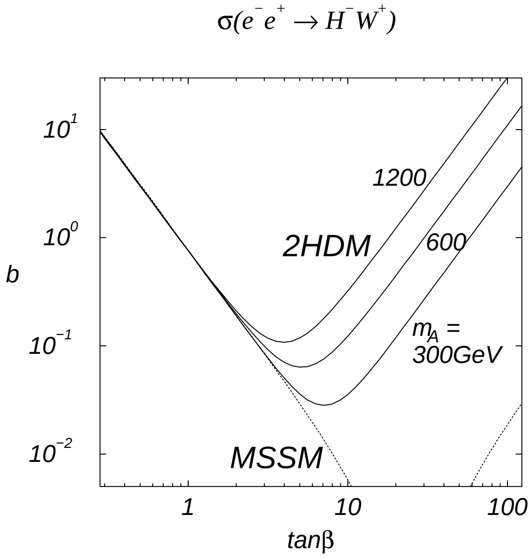


**Fig. 3.** The total cross section of $e^+e^- \to H^-W^+$ for $m_{H^\pm} = 200\,\mathrm{GeV}$ at $s^{1/2} = 500\,\mathrm{GeV}$ as a function of $\tan\beta$ in the 2HDM (solid lines) and in the MSSM (dashed line). For the 2HDM, three solid curves correspond to $m_{A^0} = 300$, 600 and 1200 GeV. The other parameters are chosen as $\alpha = \beta - \pi/2$, $m_{h^0} = 120\,\mathrm{GeV}$, $m_{H^0} = 210\,\mathrm{GeV}$ and $M = 0\,\mathrm{GeV}$

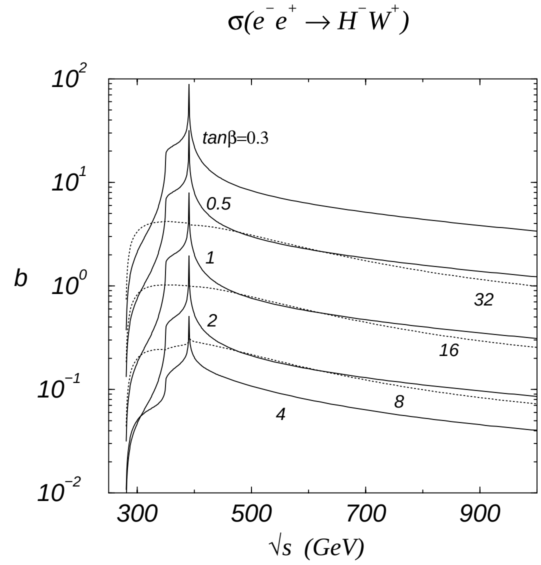


**Fig. 4.** The $s^{1/2}$ dependence of the total cross section of $e^+e^- \to H^-W^+$ for $m_{H^\pm} = 200\,\mathrm{GeV}$ for various $\tan\beta$ in the non-SUSY 2HDM. Solid curves are $\tan\beta = 0.3, 0.5, 1, 2, 4$ and dotted curves are $\tan\beta = 8, 16, 32$. The other parameters are chosen as $\alpha = \beta - \pi/2$, $m_{h^0} = 80\,\mathrm{GeV}$, $m_{H^0} = 210\,\mathrm{GeV}$, $m_{A^0} = 1200\,\mathrm{GeV}$ and $M = 0\,\mathrm{GeV}$

the condition (35) in Fig. 3 (and in Fig. 4) just to concentrate on showing the behavior of the non-decoupling effects more clearly. The results in which both the conditions (34) and (35) are included will be shown soon in Figs. 5 and 6. In Fig. 3, the real curves represent the total cross sections in the non-SUSY 2HDM for each value of $m_{A^0}$. The other parameters are taken as $m_{h^0} = 120\,\mathrm{GeV}$, $m_{H^0} = 210\,\mathrm{GeV}$, $\alpha = \beta - \pi/2$ and $M = 0$. The dotted curve represents the cross section in the MSSM with superheavy superpartner particles. For small $\tan\beta$ ($\ll (m_t/m_b)^{1/2}$), as we discussed in the previous section, the cross section is enhanced by the $t$–$b$ loop contributions both in the MSSM and in the non-SUSY 2HDM. On the other hand, for large $\tan\beta$ ($\gg (m_t/m_b)^{1/2}$), the MSSM cross section is reduced rapidly, while the Higgs non-decoupling effects enlarge the non-SUSY 2HDM cross section. For larger $m_A$, larger cross sections are observed. Our result in the MSSM here is consistent with that in [24].

Figure 4 shows the $s^{1/2}$ dependence of the total cross section in the non-SUSY 2HDM at $m_{H^\pm} = 200\,\mathrm{GeV}$ for various $\tan\beta$; the other parameters are chosen as $m_{h^0} = 120\,\mathrm{GeV}$, $m_{H^0} = 210\,\mathrm{GeV}$, $m_{A^0} = 1200\,\mathrm{GeV}$ and $\alpha = \beta - \pi/2$ and $M = 0$. The condition (35) is switched off in this figure too.

The enhancement of the cross section essentially depends on the size of the $H^\pm tb$ and $H^\pm H^\mp H^0$ coupling constants. By taking these couplings as large as possible under the conditions (34) and (35) and also under the experimental constraints mentioned before, we obtain upper bounds of the cross section in the non-SUSY 2HDM for each value of $m_{H^\pm}$ and $\tan\beta$. The situation is described in Fig. 5. The dotted curve represents the cross section with $M = 0$ at

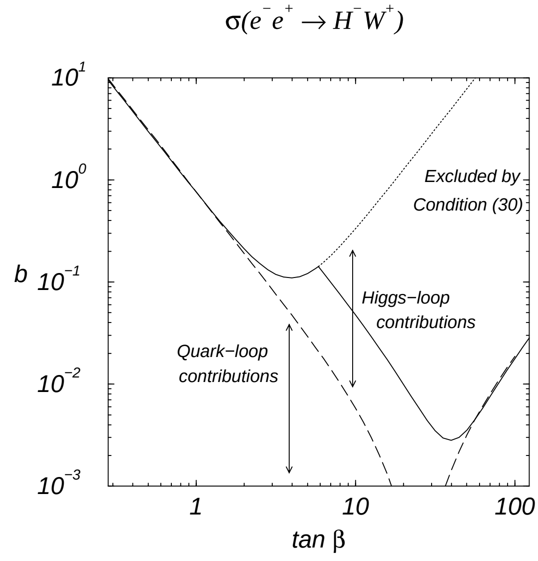


**Fig. 5.** The upper bound of the cross section of $e^+e^- \to H^-W^+$ for $m_{H^\pm} = 200\,\mathrm{GeV}$ at $s^{1/2} = 500\,\mathrm{GeV}$ as a function of $\tan\beta$ under the conditions (34) and (35) in the non-SUSY 2HDM (solid curve). The dotted curve represent the cross section where the condition (35) is switched off. The dashed curve represent the cross section where only $t$–$b$ loop contributions are included

$s^{1/2} = 500\,\mathrm{GeV}$ for $m_{H^\pm} = 200\,\mathrm{GeV}$ at $\alpha = \beta - \pi/2$, and all the other free parameters in the Higgs sector are chosen in order to obtain maximum Higgs non-decoupling effects under all the conditions[8]. For $\tan\beta \gtrsim 5.9$, the condition

[8] The other choice of $\alpha$ leads to less Higgs effects for $\tan\beta > 1$ in this case

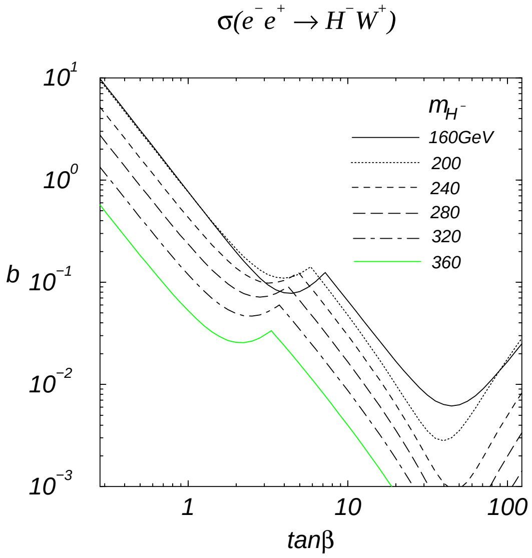


**Fig. 6.** The possible enhancement of the total cross section of $e^+e^- \to H^-W^+$ for various $m_{H^\pm}$ at $s^{1/2} = 500\,\mathrm{GeV}$ as a function of $\tan\beta$ in the non-SUSY 2HDM under the conditions (34) and (35)

(36) obtained from (35) cannot be satisfied any more if we keep $M = 0$: a larger value of $\tan\beta$ is allowed only by introducing a non-zero soft-breaking mass $M$. This leads to a smaller cross section because the non-decoupling property of the Higgs sector is weakened by a non-zero $M$: see the discussion in Sect. 4. Therefore the upper bounds are obtained as the solid curve. The cross section rapidly reduces for $\tan\beta \gtrsim 5.9$. Although the quark-loop contributions (the bottom-mass effects) enhance the cross section for $\tan\beta \gtrsim 40$, the magnitude is still much less than that for small $\tan\beta$.

In Fig. 6 we show such general bounds of the cross section as a function of $\tan\beta$ at $s^{1/2} = 500\,\mathrm{GeV}$ for $m_{H^\pm} = 160, 200, 240, 280, 320$ and $360\,\mathrm{GeV}$. All the other free parameters are chosen in the same way as in Fig. 5. Each peak of the cross section in the moderate $\tan\beta$ value is the point where the largest Higgs non-decoupling effects with $M = 0$ appear.

## 6 Discussion and conclusion

We have discussed the $H^\pm$ production process via $e^+e^- \to H^\pm W^\mp$ in the non-SUSY 2HDM as well as in the MSSM.

In the non-SUSY 2HDM, a large cross section is possible for small $\tan\beta$ by the $t$–$b$ loop contributions (quadratic top-mass effects). At $\tan\beta = 0.3$, for $m_{H^\pm} = 200\,\mathrm{GeV}$, the cross section can be as large as 8 fb at $s^{1/2} = 500\,\mathrm{GeV}$ and maximally it reaches to over 40 fb at $s^{1/2} \sim 390\,\mathrm{GeV}$. For larger $\tan\beta$, these top-mass effects decrease until $\tan\beta \sim m_t/m_b = 35$. In Model II, the quadratic bottom-mass effects enhance the cross section for $\tan\beta \gtrsim m_t/m_b$, but the magnitude is not so large: at $s^{1/2} = 500\,\mathrm{GeV}$ it is at most a few times $10^{-2}$ fb even for $\tan\beta \sim 100$. If Model I is assumed, this small enhancement for $\tan\beta > m_t/m_b$ disappears, but all the results for smaller $\tan\beta$ are almost the same as those in Model II.

In addition to the quark-loop effects, the Higgs non-decoupling effects contribute to the cross section by a few times 0.1 fb for moderate values of $\tan\beta$. Such Higgs effects are strongly bounded for larger $\tan\beta$ ($\gtrsim (m_t/m_b)^{1/2}$) by the requirement of the validity of perturbation theory.

In the MSSM with heavy superpartner particles, the Higgs-loop effects are very small and only the $t$–$b$ loops contribute to the cross section. For $m_{H^\pm} = 200\,\mathrm{GeV}$, the cross section at $\tan\beta = 2$ amounts to a few times 0.1 fb at $s^{1/2} = 500\,\mathrm{GeV}$, and maximally it reaches to over 1 fb at $s^{1/2} \sim 390\,\mathrm{GeV}$. The cross section rapidly decreases for larger $\tan\beta$. We here have not discussed the one-loop contributions of the superpartner particles in the MSSM explicitly, which will be discussed in a future paper.

We give some comments on our analysis. First, our results have been tested in the high-energy limit by using the equivalence theorem [25] at the one-loop level [26]. We evaluated $e^-e^+ \to H^-w^+$ ($w^+$ is for the charged Goldstone boson) and confirmed that the cross section was coincident with our prediction for the $H^-W_L^+$ production in the high-energy limit. Second, although the process is one-loop induced so the ultraviolet divergences have canceled among the diagrams, we have include the finite renormalization effects of the $WH$ mixing and the $wH$ mixing by putting the renormalization conditions on the mass shell of $H^\pm$. The effects have turned out to give a few% (at most about 5%) of corrections to the one-loop-induced cross sections in which the finite renormalization effects ($\delta F_{i,\tau}$) are not included.

Finally, we comment on the detectability of the signal events for the case of $m_{H^\pm} > m_t + m_b$. The $H^\pm$ decays into a $tb$-pair and the signal process is $e^+e^- \to H^\pm W^\mp \to t\bar{b}W^- + \bar{t}bW^+$. The main background process may be $e^+e^- \to t\bar{t} \to t\bar{b}W^- + \bar{t}bW^+$. The cross section of $e^+e^- \to t\bar{t}$ amounts to about 0.57 pb for $s^{1/2} = 500\,\mathrm{GeV}$: the signal/background ratio is at most around 1%. It may however be expected that the signal can be comfortably seen if the signal cross section is 10 fb, by attaining a background reduction in [27] by the following method:
(1) a cut around the reconstructed $bW$ masses which can come from the $bW$ decay at 175 GeV,
(2) find a peak in the reconstructed $m_{H^\pm}$ and
(3) confirm the presence of $H^\pm$ according to the method in [28]. For smaller signal cross sections of the order of 0.1 fb, details of the background analysis are needed to see the detectability.

### Note added in proof

After this work was finished, another paper (see [29]) appeared in which the same subject was studied.

*Acknowledgements.* The author would like to thank W. Hollik for useful discussions, K. Odagiri for valuable discussions on the backgrounds and the detectability at LC, and Y. Okada for useful information about the constraint on $\tan\beta$. This work was supported, in part, by the Alexander von Humboldt Foundation.

## A Analytic results

In the formulas below, we use the integral functions introduced by Passarino and Veltman [30]. The notation for the tensor coefficients here is based on [16]. We here write $A(m_f)$ as $A[f]$, $B_{ij}(p_H^2; m_{f_1}, m_{f_2})$ as $B_{ij}[f_1, f_2]$, $C_{ij}(p_H^2, p_W^2, p_V^2; m_{f_1}, m_{f_2}, m_{f_3})$ as $C_{ij}[f_1, f_2, f_3]$, where $f_i$ are the fields with mass $m_{f_i}$. For the quark diagrams, we define the abbreviation $C_{ij}(tbb) = C_{ij}(p_H^2, p_W^2, p_V^2; m_t, m_b, m_b)$ and $C_{ij}(ttb) = C_{ij}(p_H^2, p_V^2, p_W^2; m_t, m_t, m_b)$. The expression is in the 't Hooft–Feynman gauge. Also $J(\alpha,\beta)$, $K(\alpha,\beta)$ and $L(\alpha,\beta)$ in (31)–(33) are written as $J_{\alpha\beta}$, $K_{\alpha\beta}$ and $L_{\alpha\beta}$, and we also write

$$\tilde{K}_{\alpha\beta} = \left\{ K_{\alpha\beta}(m_{H^0}^2 - M^2) - J_{\alpha\beta}(2m_{H^\pm}^2 - m_{H^0}^2) \right\}, \quad (37)$$

$$\tilde{L}_{\alpha\beta} = \left\{ L_{\alpha\beta}(m_{H^0}^2 - M^2) + J_{\alpha\beta}(2m_{H^\pm}^2 - m_{h^0}^2) \right\}, \quad (38)$$

respectively, for brevity. The momentum squared of the $H^+$ is set on mass shell, $p_H^2 = m_{H^\pm}^2$.

### A.1 Form factors of the $H^+W^-V^0$ ($V^0 = Z^0, \gamma$) vertices

We write each contribution to the unrenormalized $H^\pm W^\mp V^0$ form factors $X^{HWV}$ ($X = F, G$ and $H$) as $X^{HWV} = X^{HWV(\mathrm{a})} + X^{HWV(\mathrm{b})} + X^{HWV(\mathrm{c})}$ corresponding to Figs. 7a,b,c. $X^{HWV(\mathrm{a})}$ is the contribution of the triangle-type diagrams (Fig. 7a), $X^{HWV(\mathrm{b})}$ represents that from the two-point function correction shown in Fig. 7b, and $X^{HWV(\mathrm{c})}$ is the tadpole contribution as well as some two-point function corrections written only by the $A$ function (Fig. 7c).

#### A.1.1 The $H^+W^-Z^0$ vertex

The contribution of triangle-type diagrams to $F^{HWZ}$ is calculated as

$$\begin{aligned}
&F^{HWZ(\mathrm{a})}(m_{H^\pm}^2, p_W^2, p_Z^2) = \frac{2}{16\pi^2 v^2 c_W} \\
&\times \Big[ -\tilde{K}_{\alpha\beta} \left\{ C_{24}[H^\pm A^0 H^0] - c_{2W} C_{24}[H^0 H^\pm H^\pm] \right\} \\
&-\tilde{L}_{\alpha\beta} \left\{ C_{24}[H^\pm A^0 h^0] - c_{2W} C_{24}[h^0 H^\pm H^\pm] \right\} \\
&+J_{\alpha\beta} \big\{ (m_{H^\pm}^2 - m_{H^0}^2) C_{24} \big( [w^\pm z^0 H^0] \\
&-c_{2W}[H^0 w^\pm w^\pm] \big) - (m_{H^\pm}^2 - m_{A^0}^2) C_{24}[w^\pm H^0 A^0] \\
&-m_W^2 C_{24}[W^\pm H^0 A^0] - \frac{c_{2W}}{c_W} m_W^2 C_{24}[H^\pm H^0 Z^0] \\
&-m_W^2 \big( 4(p_W^2 + p_W \cdot p_Z) C_0 + 2(2p_W + p_Z) \\
&\cdot (p_W C_{11} + p_Z C_{12}) + p_W \cdot p_Z C_{23} \\
&+(D-1) C_{24} \big) [W^\pm Z^0 H^0] + c_W^2 m_W^2 \big( (p_Z^2 - p_W^2) C_0 \\
&-2p_Z \cdot (p_W C_{11} + p_Z C_{12}) + p_W \cdot p_Z C_{23} \\
&+(D-1) C_{24} \big) [H^0 W^\pm W^\pm] \\
&-m_Z^2 (m_{H^\pm}^2 - m_{H^0}^2) s_W^2 C_0 [w^\pm Z^0 H^0] \\
&-m_W^2 (m_{H^\pm}^2 - m_{H^0}^2) s_W^2 C_0 [H^0 W^\pm w^\pm] \\
&+m_W^2 s_W^2 C_{24}[H^0 w^\pm W^\pm] - (H^0 \to h^0) \big\} \Big] \\
&+\frac{4N_c}{16\pi^2 v^2 c_W} \big[ m_b^2 \tan\beta \left\{ (-s_W^2 Q_b) \left( p_W \cdot (p_W + p_Z) C_{11} \right.\right. \\
&+p_Z \cdot (p_W + p_Z) C_{12} + p_W^2 C_{21} + p_Z^2 C_{22} \\
&+ 2p_W \cdot p_Z C_{23} + D C_{24} \big) (tbb) - (T_b - s_W^2 Q_b) \\
&\big( p_W^2 C_{11} + p_Z \cdot p_Z C_{12} + p_W^2 C_{21} + p_Z^2 C_{22} + 2p_W \cdot p_Z C_{23} \\
&+ (D-2) C_{24} \big) (tbb) - (T_t - s_W^2 Q_t) \\
&\big( p_Z^2 C_{11} + p_Z \cdot p_Z C_{12} + p_Z^2 C_{21} + p_W^2 C_{22} \\
&+2p_W \cdot p_Z C_{23} + (D-2) C_{24} \big) (ttb) \\
&+(-s_W^2 Q_t) m_t^2 C_0(ttb) \big\} \\
&+m_t^2 \cot\beta \big\{ -(T_b - s_W^2 Q_b) \big( (p_W^2 + p_W \cdot p_Z) C_0 \\
&+(2p_W^2 + p_W \cdot p_Z) C_{11} + (p_Z^2 + 2p_W \cdot p_Z) C_{12} \\
&+p_W^2 C_{21} + p_Z^2 C_{22} + 2p_W \cdot p_Z C_{23} + (D-2) C_{24} \big) (tbb) \\
&+(-s_W^2 Q_b) m_b^2 C_0(tbb) + (-s_W^2 Q_t) \big( p_Z \cdot (p_W + p_Z) C_{11} \\
&+p_W \cdot (p_W + p_Z) C_{12} + p_Z^2 C_{21} + p_W^2 C_{22} \\
&+ 2p_W \cdot p_Z C_{23} + D C_{24} \big) (ttb) - (T_t - s_W^2 Q_t) \\
&\times \big( (p_Z^2 + p_W \cdot p_Z) C_0 + (2p_Z^2 + p_W \cdot p_Z) C_{11} \\
&+(p_W^2 + 2p_W \cdot p_Z) C_{12} + p_Z^2 C_{21} + p_W^2 C_{22} \\
&+2p_W \cdot p_Z C_{23} + 2C_{24} \big) (ttb) \big]. \qquad (39)
\end{aligned}$$

The contribution of the diagrams expressed in terms of the $B_i$ functions is given by

$$\begin{aligned}
&F^{HWZ(\mathrm{b})}(m_{H^\pm}^2, p_W^2, p_Z^2) = \frac{2}{16\pi^2 v^2 c_W} \\
&\times \Bigg[ \frac{1}{2} \tilde{K}_{\alpha\beta} \Big\{ s_W^2 B_0[H^0 H^\pm] \\
&+\frac{p_Z^2 - p_W^2}{m_{H^\pm}^2 - m_W^2} c_W^2 (B_0 + 2B_1)[H^0 H^\pm] \\
&+\frac{m_{H^0}^2 - m_{H^\pm}^2}{m_{H^\pm}^2 - m_W^2} s_W^2 B_0[H^0 H^\pm] \Big\} + \frac{1}{2} \tilde{L}_{\alpha\beta} \Big\{ s_W^2 B_0[h^0 H^\pm] \\
&+\frac{p_Z^2 - p_W^2}{m_{H^\pm}^2 - m_W^2} c_W^2 (B_0 + 2B_1)[h^0 H^\pm] \\
&+\frac{m_{h^0}^2 - m_{H^\pm}^2}{m_{H^\pm}^2 - m_W^2} s_W^2 B_0[h^0 H^\pm] \Big\} \\
&+\frac{1}{2} J_{\alpha\beta} \big\{ -(m_{H^\pm}^2 - m_{H^0}^2) s_W^2 B_0[H^0 w^\pm] \\
&+m_W^2 s_W^2 B_0(p_W^2; W^\pm H^0) + m_Z^2 s_W^2 B_0 B_0(p_Z^2; Z^0 H^0) \\
&-\frac{1}{2} \frac{m_W^2}{m_{H^\pm}^2 - m_W^2} s_W^2 \\
&\times \left\{ m_{H^\pm}^2 (B_0 - 2B_1 + B_{21}) + D B_{22} \right\} [H^0 W^\pm] \\
&+\frac{1}{2} m_{H^0}^2 \frac{m_{H^0}^2 - m_{H^\pm}^2}{m_{H^\pm}^2 - m_W^2} s_W^2 B_0[H^0 w^\pm]
\end{aligned}$$

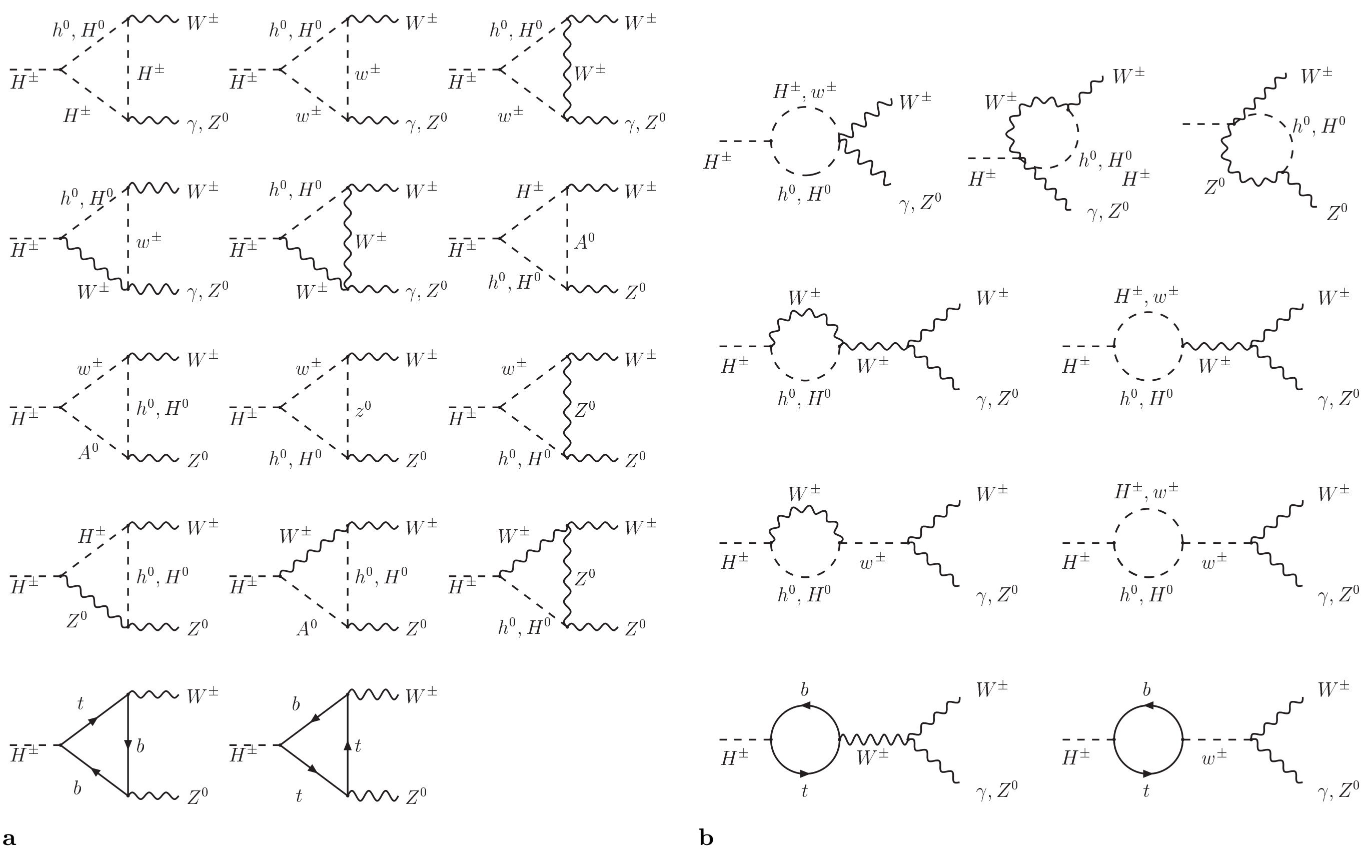


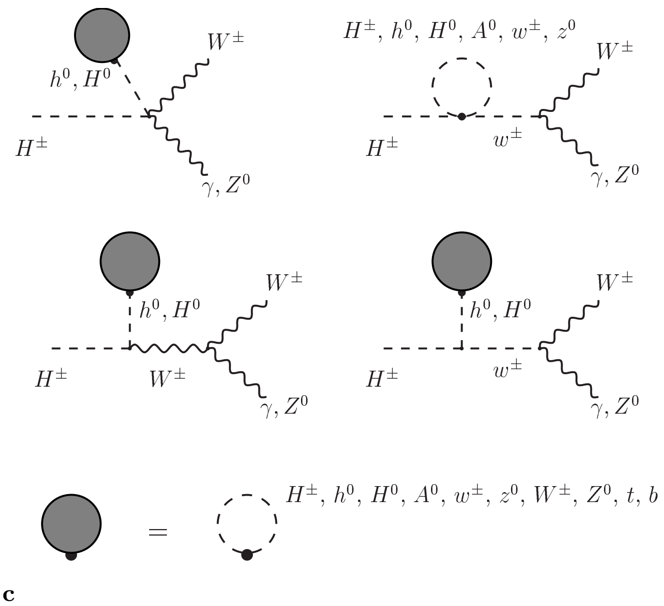


**Fig. 7.** **a** The first group of the Feynman diagrams (the 't Hooft–Feynman gauge) of the $HWV$ vertices ($V = \gamma, Z^0$), which corresponds to $X^{HWV(\mathrm{a})}$ ($X = F, G$ and $H$) in Appendix A.1. **b** The second group of the Feynman diagrams (the 't Hooft–Feynman gauge) of the $HWV$ vertices ($V = \gamma, Z^0$), which corresponds to $X^{HWV(\mathrm{b})}$ ($X = F, G$ and $H$) in Appendix A.1. **c** The third group of the Feynman diagrams (the 't Hooft–Feynman gauge) of the $HWV$ vertices ($V = \gamma, Z^0$), which corresponds to $X^{HWV(\mathrm{c})}$ ($X = F, G$ and $H$) in Appendix A.1

$$
\begin{aligned}
&+m_W^2 \frac{p_Z^2 - p_W^2}{m_{H^\pm}^2 - m_W^2} c_W^2 (B_0 - B_1)[H^0 W^\pm] \\
&+\frac{m_{H^0}^2 - m_{H^\pm}^2}{m_{H^\pm}^2 - m_W^2}(p_Z^2 - p_W^2) c_W^2 (B_0 + 2B_1)[H^0 w^\pm] \\
&-(H^0 \to h^0)\}] \\
&+\frac{4N_c}{16\pi^2 v^2 c_W}\left[\frac{s_W^2}{m_{H^\pm}^2 - m_W^2}\left\{(m_b^2 \tan\beta - m_t^2 \cot\beta)\right.\right. \\
&\times \left(m_{H^\pm}^2 (B_1 + B_{21}) + D B_{22}\right)[tb] \\
&\left. -m_t^2 m_b^2 (\tan\beta - \cot\beta) B_0 [tb]\right\} \\
&-\frac{c_W^2}{m_{H^\pm}^2 - m_W^2}(p_Z^2 - p_W^2) \\
&\left.\times \left\{m_b^2 \tan\beta B_1 + m_t^2 \cot\beta (B_1 + B_0)\right\}[tb]\right]. \qquad (40)
\end{aligned}
$$

The diagrams relevant to the $A$ function are expressed by

$$F^{HWZ(\mathrm{c})}(m_{H^\pm}^2, p_W^2, p_Z^2) = \frac{1}{16\pi^2 v^2 c_W} \frac{1}{m_{H^\pm}^2 - m_W^2}$$
$$\times \left[ s_W^2 \left( \tilde{\Pi}_{Hw}^B - T_1 \right) - \left\{ s_W^2 m_W^2 - c_W^2 (p_Z^2 - m_W^2) \right\} T_2 \right], \tag{41}$$

where $\tilde{\Pi}_{Hw}^B$, $T_1$ and $T_2$ are given in (57), (58) and (55).

The contribution of the triangle-type diagrams to $G^{HWZ}$ and $H^{HWZ}$ are given by

$$G^{HWZ(\mathrm{a})}(m_{H^\pm}^2, p_W^2, p_Z^2) = \frac{2m_W^2}{16\pi^2 v^2 c_W}$$
$$\times \Big[ -\tilde{K}_{\alpha\beta}(C_{12}+C_{23}) \left\{ [H^\pm A^0 H^0] - c_{2W}[H^0 H^\pm H^\pm] \right\}$$
$$-\tilde{L}_{\alpha\beta}(C_{12}+C_{23}) \left\{ [H^\pm A^0 h^0] - c_{2W}[h^0 H^\pm H^\pm] \right\}$$
$$+J_{\alpha\beta} \left\{ (m_{H^\pm}^2 - m_{H^0}^2)(C_{12}+C_{23})[w^\pm z^0 H^0] \right.$$
$$-(m_{H^\pm}^2 - m_{H^0}^2) c_{2W} (C_{12}+C_{23})[H^0 w^\pm w^\pm]$$
$$-(m_{H^\pm}^2 - m_{A^0}^2)(C_{12}+C_{23})[w^\pm H^0 A^0]$$
$$-m_W^2 (2C_0 + 2C_{11} + C_{12} + C_{23}) [W^\pm H^0 A^0]$$
$$-\frac{c_{2W}}{c_W} m_W^2 (-C_{12}+C_{23})[H^\pm H^0 Z^0]$$
$$+m_W^2 (2C_0 - 2C_{11} + 5C_{12} + C_{23}) [W^\pm Z^0 H^0]$$
$$+c_W^2 m_W^2 (4C_{11} - 3C_{12} - C_{23}) [H^0 W^\pm W^\pm]$$
$$\left. +m_W^2 s_W^2 (C_{23} - C_{12}) [H^0 w^\pm W^\pm] - (H^0 \to h^0) \right\} \Big]$$
$$+\frac{4N_c m_W^2}{16\pi^2 v^2 c_W} \Big[ m_b^2 \tan\beta \left\{ (-s_W^2 Q_b)(C_{12} - C_{11})(tbb) \right.$$
$$+(T_b - s_W^2 Q_b)(2C_{23} + C_{12})(tbb)$$
$$\left. +(T_t - s_W^2 Q_t)(C_{12} + 2C_{23})(tbb) \right\}$$
$$+m_t^2 \cot\beta \left\{ (T_b - s_W^2 Q_b)(C_0 + C_{11} + 2C_{12} + 2C_{23})(tbb) \right.$$
$$-(-s_W^2 Q_t)(C_{11} - C_{12})(ttb)$$
$$\left. +(T_t - s_W^2 Q_t)(C_0 + C_{11} + 2C_{12} + 2C_{23})(ttb) \right\} \Big], \tag{42}$$

$$H^{HWZ(\mathrm{a})}(m_{H^\pm}^2, p_W^2, p_Z^2) = \frac{4N_c m_W^2}{16\pi^2 v^2 c_W}$$
$$\times \Big[ m_b^2 \tan\beta (-s_W^2 Q_b) \left\{ (C_{12} - C_{11})(tbb) \right.$$
$$\left. -(T_b - s_W^2 Q_b) C_{12}(tbb) - (T_t - s_W^2 Q_t) C_{12}(ttb) \right\}$$
$$+m_t^2 \cot\beta \left\{ -(T_b - s_W^2 Q_b)(C_0 + C_{11})(tbb) \right.$$
$$\times(-s_W^2 Q_t)(C_{11} - C_{12})(ttb)$$
$$\left. -(T_t - s_W^2 Q_t)(C_0 + C_{11})(ttb) \right\} \Big]. \tag{43}$$

There is no contribution from the other diagrams to $G^{HWZ}$ and $H^{HWZ}$:

$$G^{HWZ(\mathrm{b})} = G^{HWZ(\mathrm{c})} = H^{HWZ(\mathrm{b,c})} = 0. \tag{44}$$

### A.1.2 The $H^+W^-\gamma$ vertex

By making the similar decomposition to the $HWZ$ vertex, we obtain contributions of the $H^+W^-\gamma$ vertex to each form factor.

$$F^{HW\gamma(\mathrm{a})}(m_{H^\pm}^2, p_W^2, p_\gamma^2) = \frac{4s_W}{16\pi^2 v^2} \Big[ \tilde{K}_{\alpha\beta} C_{24}[H^0 H^\pm H^\pm]$$
$$+\tilde{L}_{\alpha\beta} C_{24}[h^0 H^\pm H^\pm]$$
$$+J_{\alpha\beta} \left\{ \frac{m_W^2}{2} \left( (p_\gamma^2 - p_W^2) C_0 - 2p_\gamma \cdot (p_W C_{11} + p_\gamma C_{12}) \right. \right.$$
$$\left. +p_W \cdot p_\gamma C_{23} + (D-1) C_{24} \right) [H^0 W^\pm W^\pm]$$
$$+\frac{m_W^2}{2} (m_{H^\pm}^2 - m_{H^0}^2) C_0 [H^0 W^\pm w^\pm]$$
$$-\frac{m_W^2}{2} C_{24} [H^0 w^\pm W^\pm] - (m_{H^\pm}^2 - m_{H^0}^2) C_{24} [H^0 w^\pm w^\pm]$$
$$\left. -(H^0 \to h^0) \right\} \Big]$$
$$+\frac{4s_W N_c}{16\pi^2 v^2} \Big[ m_b^2 \tan\beta \left\{ Q_b \left( p_W \cdot (p_W + p_\gamma) C_{11} \right. \right.$$
$$+p_\gamma \cdot (p_W + p_\gamma) C_{12} + p_W^2 C_{21} + p_\gamma^2 C_{22}$$
$$\left. +2p_W \cdot p_\gamma C_{23} + 4C_{24} \right) (tbb)$$
$$-Q_b \left( p_W^2 C_{11} + p_W \cdot p_\gamma C_{12} + p_W^2 C_{21} + p_\gamma^2 C_{22} \right.$$
$$\left. +2p_W \cdot p_\gamma C_{23} + 2C_{24} \right) (tbb)$$
$$-m_b^2 \tan\beta Q_t \left( p_\gamma^2 C_{11} + p_\gamma \cdot p_Z C_{12} + p_\gamma^2 C_{21} + p_W^2 C_{22} \right.$$
$$\left. \left. +2p_W \cdot p_\gamma C_{23} + 2C_{24} \right) (ttb) + m_t^2 Q_t C_0 (ttb) \right\}$$
$$+m_t^2 \cot\beta \left\{ -Q_b \left( (p_W^2 + p_W \cdot p_\gamma) C_0 \right. \right.$$
$$+(2p_W^2 + p_W \cdot p_\gamma) C_{11} + (p_\gamma^2 + 2p_W \cdot p_\gamma) C_{12}$$
$$+p_W^2 C_{21} + p_\gamma^2 C_{22}$$
$$\left. +2p_W \cdot p_\gamma C_{23} + 2C_{24} \right) (tbb) + m_b^2 Q_b C_0 (tbb)$$
$$+Q_t \left( p_\gamma \cdot (p_W + p_\gamma) C_{11} + p_W \cdot (p_W + p_\gamma) C_{12} \right.$$
$$\left. +p_\gamma^2 C_{21} + p_W^2 C_{22} + 2p_W \cdot p_\gamma C_{23} + 4C_{24} \right) (ttb)$$
$$-Q_t \left( (p_\gamma^2 + p_W \cdot p_\gamma) C_0 + (2p_\gamma^2 + p_W \cdot p_\gamma) C_{11} \right.$$
$$+(p_W^2 + 2p_W \cdot p_\gamma) C_{12} + p_\gamma^2 C_{21} + p_W^2 C_{22}$$
$$\left. +2p_W \cdot p_\gamma C_{23} + 2C_{24} \right) (ttb) \Big], \tag{45}$$

$$F^{HW\gamma(\mathrm{b})}(m_{H^\pm}^2, p_W^2, p_\gamma^2) = \frac{4s_W}{16\pi^2 v^2}$$
$$\times \Big[ -\frac{1}{4} \tilde{K}_{\alpha\beta} \left\{ B_0[H^0 H^\pm] + \frac{m_{H^0}^2 - m_{H^\pm}^2}{m_{H^\pm}^2 - m_W^2} B_0[H^0 H^\pm] \right.$$
$$\left. - \frac{p_\gamma^2 - p_W^2}{m_{H^\pm}^2 - m_W^2} (B_0 + 2B_1)[H^0 H^\pm] \right\}$$
$$-\frac{1}{4} \tilde{L}_{\alpha\beta} \left\{ B_0[h^0 H^\pm] + \frac{m_{h^0}^2 - m_{H^\pm}^2}{m_{H^\pm}^2 - m_W^2} B_0[h^0 H^\pm] \right.$$
$$\left. - \frac{p_\gamma^2 - p_W^2}{m_{H^\pm}^2 - m_W^2} (B_0 + 2B_1)[h^0 H^\pm] \right\}$$

$$+J_{\alpha\beta}\left\{\frac{1}{4}(m_{H^\pm}^2 - m_{H^0}^2)B_0[H^0 w^\pm] - \frac{m_W^2}{2}B_0(p_W^2; W^\pm H^0)\right.$$
$$+\frac{1}{4}\frac{m_W^2}{m_{H^\pm}^2 - m_W^2}$$
$$\times\left\{m_{H^\pm}^2(B_0 - 2B_1 + B_{21}) + DB_{22}\right\}[H^0 W^\pm]$$
$$-\frac{m_{H^0}^2}{4}\frac{m_{H^0}^2 - m_{H^\pm}^2}{m_{H^\pm}^2 - m_W^2}B_0[H^0 w^\pm]$$
$$+\frac{1}{2}\frac{m_{H^0}^2 - m_{H^\pm}^2}{m_{H^\pm}^2 - m_W^2}(p_\gamma^2 - p_W^2)(B_0 + 2B_1)[H^0 w^\pm]$$
$$\left.\left.+\frac{m_W^2}{2}\frac{p_\gamma^2 - p_W^2}{m_{H^\pm}^2 - m_W^2}(B_0 - B_1)[H^0 W^\pm] - (H^0 \to h^0)\right\}\right]$$
$$+\frac{4s_W}{16\pi^2 v^2}\left[-\frac{p_\gamma^2 - p_W^2}{m_{H^\pm}^2 - m_W^2}\right.$$
$$\times\left\{m_b^2 \tan\beta B_1 + m_t^2 \cot\beta(B_1 + B_0)\right\}[tb]$$
$$-\frac{1}{m_{H^\pm}^2 - m_W^2}$$
$$\times\left\{(m_b^2 \tan\beta - m_t^2 \cot\beta)(m_{H^\pm}^2(B_1 + B_{21}) + DB_{22})\right.$$
$$\left.\left.+m_t^2 m_b^2(\tan\beta - \cot\beta)B_0\right\}[tb]\right], \tag{46}$$
$$F^{HW\gamma(\mathrm{c})}(m_{H^\pm}^2, p_W^2, p_\gamma^2) = -\frac{s_W}{16\pi^2 v^2}\frac{1}{m_{H^\pm}^2 - m_W^2}$$
$$\times\left\{\tilde{\Pi}_{Hw}^B - T_1 + (p_\gamma^2 - p_W^2 + m_W^2)T_2\right\}, \tag{47}$$

where $T_1$ and $T_2$ and $\tilde{\Pi}_{Hw}^B$ are defined in (57), (58) and (55).

$$G^{HW\gamma(\mathrm{a})}(m_{H^\pm}^2, p_W^2, p_\gamma^2) = \frac{4m_W^2 s_W}{16\pi^2 v^2}$$
$$\times\left[\tilde{K}_{\alpha\beta}(C_{12} + C_{23})[H^0 H^\pm H^\pm] + \tilde{L}_{\alpha\beta}\right.$$
$$\times(C_{12} + C_{23})[h^0 H^\pm H^\pm]$$
$$+J_{\alpha\beta}\left\{\frac{m_W^2}{2}(4C_{11} - 3C_{12} - C_{23})[H^0 W^\pm W^\pm]\right.$$
$$+\frac{m_W^2}{2}(C_{12} - C_{23})[H^0 w^\pm W^\pm]$$
$$-(m_{H^\pm}^2 - m_{H^0}^2)(C_{12} + C_{23})[H^0 w^\pm w^\pm]$$
$$\left.\left.-(H^0 \to h^0)\right\}\right]$$
$$+\frac{4m_W^2 s_W N_c}{16\pi^2 v^2}\left[m_b^2 \tan\beta Q_b(C_{12} - C_{11})(tbb)\right.$$
$$+m_b^2 \tan\beta Q_b(2C_{23} + C_{12})(tbb)$$
$$+m_t^2 \cot\beta Q_b(C_0 + C_{11} + 2C_{12} + 2C_{13})(tbb)$$
$$+m_t^2 \cot\beta Q_t$$
$$\times(C_{12} - C_{11})(ttb) + m_b^2 \tan\beta Q_t(2C_{23} + C_{12})(ttb)$$
$$\left.+m_t^2 \cot\beta Q_t(C_0 + C_{11} + 2C_{12} + 2C_{23})(ttb)\right], \tag{48}$$
$$H^{HW\gamma(\mathrm{a})}(m_{H^\pm}^2, p_W^2, p_\gamma^2) = \frac{4m_W^2 s_W N_c}{16\pi^2 v^2}$$
$$\times\left[m_b^2 \tan\beta Q_b(C_{12} - C_{11})(tbb) - m_b^2 \tan\beta Q_b C_{12}(tbb)\right.$$
$$-m_t^2 \cot\beta Q_b(C_0 + C_{11})(tbb)$$
$$+m_t^2 \cot\beta Q_t(C_{11} - C_{12})(ttb) - m_b^2 \tan\beta Q_t C_{12}(ttb)$$
$$\left.-m_t^2 \cot\beta Q_t(C_0 + C_{11})(ttb)\right] \tag{49}$$

and

$$G^{HW\gamma(\mathrm{b,c})} = H^{HW\gamma(\mathrm{b,c})} = 0. \tag{50}$$

### A.2 Tadpole diagrams and the $w$–$H$ two-point function

The tadpole graphs i$T_H$ and i$T_h$ are calculated to be

$$T_H = \frac{1}{16\pi^2 v}\left[m_{H^0}^2 \cos(\alpha-\beta)\left(A[w^\pm] + \frac{1}{2}A[z^0]\right)\right.$$
$$+\left\{\left(\frac{\cos\alpha\sin^2\beta}{\cos\beta} - \frac{\sin\alpha\cos^2\beta}{\sin\beta}\right)m_{H^0}^2\right.$$
$$\left.+2\cos(\alpha-\beta)m_{H^\pm}^2 + \frac{\sin(\alpha+\beta)}{\sin\beta\cos\beta}M^2\right\}A[H^\pm]$$
$$+\left\{\left(\frac{\cos\alpha\sin^2\beta}{\cos\beta} - \frac{\sin\alpha\cos^2\beta}{\sin\beta}\right)m_{H^0}^2\right.$$
$$\left.+2\cos(\alpha-\beta)m_{A^0}^2 + \frac{\sin(\alpha+\beta)}{\sin\beta\cos\beta}M^2\right\}\frac{1}{2}A[A^0]$$
$$+\frac{3}{2}\left\{\left(\frac{\cos^3\alpha}{\cos\beta} + \frac{\sin^3\alpha}{\sin\beta}\right)m_{H^0}^2\right.$$
$$\left.-\frac{\cos 2\beta}{\cos\beta\sin\beta}\sin(\alpha-\beta)M^2\right\}A[H^0]$$
$$+\left\{\frac{1}{2}(m_{H^0}^2 + 2m_{h^0}^2)\frac{\sin 2\alpha}{\sin 2\beta}\right.$$
$$\left.-\frac{M^2}{4\cos\beta\sin\beta}(-3\sin 2\alpha + \sin 2\beta)\right\}$$
$$\times\cos(\alpha-\beta)A[h^0]$$
$$+8\cos(\alpha-\beta)\left(m_W^2 A[W^\pm] + \frac{1}{2}m_Z^2 A[Z^0]\right)$$
$$\left.-4N_c\left(\frac{\cos\alpha}{\cos\beta}A[b] + \frac{\sin\alpha}{\sin\beta}A[t]\right)\right], \tag{51}$$
$$T_h = \frac{1}{16\pi^2 v}\left[-m_{h^0}^2 \sin(\alpha-\beta)\left(A[w^\pm] + \frac{1}{2}A[z^0]\right)\right.$$
$$+\left\{\left(\frac{\sin\alpha\sin^2\beta}{\cos\beta} - \frac{\cos\alpha\cos^2\beta}{\sin\beta}\right)m_{h^0}^2\right.$$
$$\left.-2\sin(\alpha-\beta)m_{H^\pm}^2 + \frac{\cos(\alpha+\beta)}{\sin\beta\cos\beta}M^2\right\}A[H^\pm]$$
$$+\left\{\left(\frac{\sin\alpha\sin^2\beta}{\cos\beta} - \frac{\cos\alpha\cos^2\beta}{\sin\beta}\right)m_{h^0}^2\right.$$
$$\left.-2\sin(\alpha-\beta)m_{A^0}^2 + \frac{\cos(\alpha+\beta)}{\sin\beta\cos\beta}M^2\right\}\frac{1}{2}A[A^0]$$

$$
\begin{aligned}
&-\frac{3}{2}\left\{\left(\frac{\sin^3\alpha}{\cos\beta}-\frac{\cos^3\alpha}{\sin\beta}\right)m_{h^0}^2\right.\\
&\left.+\frac{\cos 2\beta}{\cos\beta\sin\beta}\cos(\alpha-\beta)M^2\right\}A[h^0]\\
&+\frac{1}{2}\left\{(2m_{H^0}^2+m_{h^0}^2)\frac{\sin 2\alpha}{\sin 2\beta}\right.\\
&\left.-\frac{M^2}{4\cos\beta\sin\beta}(3\sin 2\alpha+\sin 2\beta)\right\}\\
&\times\sin(\alpha-\beta)A[H^0]\\
&-8\sin(\alpha-\beta)\left(m_W^2A[W^\pm]+\frac{1}{2}m_Z^2A[Z^0]\right)\\
&\left.-4N_c\left(\frac{\sin\alpha}{\cos\beta}A[b]+\frac{\cos\alpha}{\sin\beta}A[t]\right)\right]. \qquad (52)
\end{aligned}
$$

The $w$–$H$ two-point function is given by

$$
\Pi_{wH}(p^2)=\Pi_{wH}^A(p^2)+\Pi_{wH}^B+\Pi_{wH}^C, \qquad (53)
$$

where $\Pi_{wH}^B$ is the contribution of the diagrams which include a quartic Higgs self-coupling constants and $\Pi_{wH}^C$ is the tadpole contribution. The explicit formulas are

$$
\begin{aligned}
&\Pi_{Hw}^A(m_{H^\pm}^2)=\frac{1}{16\pi^2v^2}\left[(m_{H^0}^2-m_{H^\pm}^2)\tilde{K}_{\alpha\beta}B_0[H^0H^\pm]\right.\\
&+(m_{h^0}^2-m_{H^\pm}^2)\tilde{L}_{\alpha\beta}B_0[h^0H^\pm]\\
&+J_{\alpha\beta}\left\{-m_W^2\left(p^2(B_0-2B_1+B_{21})+DB_{22}\right)[H^0W^\pm]\right.\\
&\left.+m_{H^0}^2(m_{H^0}^2-m_{H^\pm}^2)B_0[H^0w^\pm]-(H^0\to h^0)\right\}\\
&+\frac{4N_c}{16\pi^2v^2}\left[(m_b^2\tan\beta-m_t^2\cot\beta)\right.\\
&\times\left(m_{H^\pm}^2(B_1+B_{21})+DB_{22}\right)[tb]\\
&\left.-m_t^2m_b^2(\tan\beta-\cot\beta)B_0[tb]\right], \qquad (54)
\end{aligned}
$$

$$
\begin{aligned}
&\Pi_{Hw}^B=\frac{1}{16\pi^2v^2}\tilde{\Pi}_{Hw}^B=\frac{1}{16\pi^2v^2}\left[2(m_{H^0}^2-m_{h^0}^2)J_{\alpha\beta}\right.\\
&\times\left(A[W^\pm]+\frac{1}{4}A[Z^0]\right)\\
&2\left\{+(K_{\alpha\beta}-J_{\alpha\beta})m_{H^0}^2+(L_{\alpha\beta}+J_{\alpha\beta})m_{h^0}^2\right.\\
&\left.-2\cot 2\beta M^2\right\}\left(A[H^\pm]+\frac{1}{4}A[A^0]\right)\\
&+J_{\alpha\beta}m_{H^\pm}^2\left(A[h^0]-A[H^0]\right)\\
&+\frac{1}{4}\sin 2\beta\left(\frac{\sin^4\alpha}{\sin^2\beta}-\frac{\cos^4\alpha}{\cos^2\beta}+\frac{\sin 2\alpha\cos 2\alpha}{\sin 2\beta}\right)m_{H^0}^2A[H^0]\\
&+\frac{1}{4}\sin 2\beta\left(\frac{\cos^4\alpha}{\sin^2\beta}-\frac{\sin^4\alpha}{\cos^2\beta}+\frac{\sin 2\alpha\cos 2\alpha}{\sin 2\beta}\right)m_{h^0}^2A[h^0]\\
&+\frac{1}{4}\sin 2\beta\left(\frac{\sin^2\alpha\cos^2\alpha}{\sin^2\beta}-\frac{\sin^2\alpha\cos^2\alpha}{\cos^2\beta}-\frac{\sin 2\alpha\cos 2\alpha}{\sin 2\beta}\right)\\
&\times\left(m_{h^0}^2A[H^0]+m_{H^0}^2A[h^0]\right)-\frac{M^2}{2}\frac{\cos 2\beta}{\cos\beta\sin\beta}\\
&\left.\times\left(\sin^2(\alpha-\beta)A[H^0]+\cos^2(\alpha-\beta)A[h^0]\right)\right], \qquad (55)
\end{aligned}
$$

$$
\Pi_{Hw}^C=\frac{1}{v}\left(-T_1+m_{H^\pm}^2T_2\right), \qquad (56)
$$

where

$$
T_1=16\pi^2v^2\left\{\sin(\alpha-\beta)T_H+\cos(\alpha-\beta)T_h\right\}, \qquad (57)
$$

$$
\begin{aligned}
T_2=16\pi^2v^2&\left\{\frac{1}{m_{H^0}^2}\sin(\alpha-\beta)T_H\right.\\
&\left.+\frac{1}{m_{h^0}^2}\cos(\alpha-\beta)T_h\right\}. \qquad (58)
\end{aligned}
$$

### A.3 The $t$ channel contribution

The contribution of the $t$ channel diagram (Fig. 1b) is only from the $W^+H^-$ mixing. When we write the $W^\mu H$ two-point function as

$$
\mathrm{i}\Pi_{WH}^\mu(p)=\mathrm{i}p^\mu\Pi_{WH}(p^2), \qquad (59)
$$

the contribution to the form factor is expressed by

$$
F_{i,\tau}^t(t)=\delta_{i,1}\delta_{\tau,-1}\frac{g^2}{2}\frac{1}{m_{H^\pm}^2-m_W^2}\Pi_{WH}(m_{H^\pm}^2). \qquad (60)
$$

where

$$
\begin{aligned}
&\Pi_{WH}(p^2)\\
&=\frac{m_W}{16\pi^2v^2}\left[\tilde{K}_{\alpha\beta}\left(2B_1+B_0\right)[H^0H^\pm]+\tilde{L}_{\alpha\beta}\left(2B_1+B_0\right)\right.\\
&\times[h^0H^\pm]+J_{\alpha\beta}\left\{2m_W^2(B_0-B_1)[H^0W^\pm]\right.\\
&\left.+(m_{H^0}^2-m_{H^\pm}^2)\left(2B_1+B_0\right)[H^0w^\pm]-(H^0\to h^0)\right\}\\
&\left.-4N_c\left\{m_b^2\tan\beta B_1+m_t^2\cot\beta(B_1+B_0)\right\}[tb]-T_2\right], \qquad (61)
\end{aligned}
$$

where the tadpole contribution $T_2$ is given in (58).

### A.4 The box diagram

The contribution from the box diagrams (Fig. 1c) is parametrized as

$$
\begin{aligned}
F_{i,\tau}^{\mathrm{box}}(s,t)=&-\frac{1}{16\pi^2}\frac{g^4}{4}m_WJ_{\alpha\beta}\left\{f_i^{\mathrm{box}}[\nu,W,H^0,W]\right.\\
&\left.-f_i^{\mathrm{box}}[\nu,W,h^0,W]\right\}\delta_{\tau,-1}. \qquad (62)
\end{aligned}
$$

The functions $f_i^{\mathrm{box}}$ are calculated as

$$
\begin{aligned}
&f_1^{\mathrm{box}}[\nu,W,S,W]\\
&=\left\{2(t-m_{H^\pm}^2)D_{11}+2m_{H^\pm}^2D_{12}+(s-m_{H^\pm}^2-m_W^2)\right.\\
&\times D_{13}+m_{H^\pm}^2D_{22}+m_W^2D_{23}+(t-m_{H^\pm}^2)D_{24}\\
&+(-s-t+m_{H^\pm}^2)D_{25}+(s-m_{H^\pm}^2-m_W^2)D_{26}\\
&\left.+4D_{27}\right\}[\nu,W,S,W], \qquad (63)
\end{aligned}
$$

$$f_2^{\rm box}[\nu, W, S, W] = m_W^2 D_{13}[\nu, W, S, W], \quad (64)$$

$$f_3^{\rm box}[\nu, W, S, W] = m_W^2 \left(\frac{1}{2}D_{11} + D_{13}\right)[\nu, W, S, W], \quad (65)$$

where

$$D_{ij}[\nu, W, S, W] = D_{ij}\left(k^2, p_H^2, p_W^2, \overline{k}^2; 0, m_W, m_S, m_W\right), \quad (S = h^0, H^0). \quad (66)$$

### A.5 Finite renormalization effects

The counterterm in (20) is obtained in terms of Re $\left(\Pi_{HW}(m_{H^\pm}^2)\right)$ and Re $\left(\Pi_{Hw}(m_{H^\pm}^2)\right)$. We decompose $\delta F_{i,\tau}$ into three parts as similarly to the one-loop diagram part in (20),

$$\delta F_{i,\tau}(s,t) = \delta F_{i,\tau}^Z(s) + \delta F_{i,\tau}^\gamma(s) + \delta F_{i,\tau}^t(t). \quad (67)$$

where each part in RHS is written

$$\delta F_{i,\tau}^V(s) = \delta_{i,1} g m_W C_V \frac{1}{s - m_V^2} \delta F^{HWV} \times \left(m_W^2, s, m_{H^\pm}^2\right), \quad (68)$$

$$\delta F_{i,\tau}^t(t) = -\delta_{i,1}\delta_{\tau,-1}\frac{g^2}{2(m_{H^\pm}^2 - m_W^2)} \times {\rm Re}\left(\Pi_{WH}(m_{H^\pm}^2)\right), \quad (69)$$

where $V$ represents $Z$ or $\gamma$, and $F^{HWV}(m_W^2, m_Z^2)$ and $F_{i,\tau}^t$ are expressed by

$$\delta F^{HWZ}(p_W^2, p_Z^2, m_{H^\pm}^2) = \frac{1}{c_W}\left(c_W^2 \frac{p_W^2 - p_Z^2}{m_{H^\pm}^2 - m_W^2} - s_W^2\right)\frac{1}{m_W}{\rm Re}\left(\Pi_{WH}(m_{H^\pm}^2)\right) - \frac{1}{c_W}\frac{s_W^2 m_{H^\pm}^2}{m_{H^\pm}^2 - m_W^2}{\rm Re}\left(\Pi_{wH}(m_{H^\pm}^2)\right), \quad (70)$$

$$\delta F^{HW\gamma}(p_W^2, p_\gamma^2, m_{H^\pm}^2) = s_W\left(1 + \frac{p_W^2 - p_\gamma^2}{m_{H^\pm}^2 - m_W^2}\right)\frac{1}{m_W}{\rm Re}\left(\Pi_{WH}(m_{H^\pm}^2)\right) + \frac{s_W}{m_{H^\pm}^2 - m_W^2}{\rm Re}\left(\Pi_{wH}(m_{H^\pm}^2)\right), \quad (71)$$

where $\Pi_{wH}(p^2)$ and $\Pi_{WH}(p^2)$ are given in (53) and (61).

## References


1. JLC-1, KEK Report 92-16 (1992); Physics and Technology of the Next Linear Collider: a Report submitted to Snowmass 1996, BNL 52-502, FNAL-PUB-96/112, LBNL-PUB-5425, SLAC Report 485, UCRL-ID-124160; TESLA TECHNICAL DESIGN REPORT: Physics and Detector (http://www.desy.de/˜behnke/tdr/Welcome.html)
2. A. Méndez, A. Pomarol, Nucl. Phys. B **349**, 369 (1991)
3. M. Capdequi Peyranère, H.E. Haber, P. Irulegui, Phys. Rev. D **44**, 191 (1991)
4. S. Kanemura, Phys. Rev. D **61**, 095001 (2000)
5. A. Arhrib, M. Capdequi Peyranère, G. Moultaka, Phys. Lett. B **341**, 313 (1995); J. Guasch, W. Hollik, A. Kraft, Talk at the Vth workshop in the 2nd ECFA/DESY Study on Physics and Detectors For a Linear Electron-Positron Collider, Obernai (France) 16–19th October 1999 (hep-ph/9911452)
6. T. Appelquist, J. Carazzone, Phys. Rev. D **11**, 2856 (1975)
7. S. Kanemura, T. Kasai, Y. Okada, Phys. Lett. B **471**, 182 (1999)
8. P. Ciafaloni, D. Esprin, Phys. Rev. D **56**, 1752 (1997); S. Kanemura, H-A. Tohyama, Phys. Rev. D **57**, 2949 (1998)
9. H. Hüffel, G. Pocsik, Z. Phys. C **8**, 13 (1981); J. Maalampi, J. Sirkka, I. Vilja, Phys. Lett. B **265**, 371 (1991); S. Kanemura, T. Kubota, E. Takasugi, Phys. Lett. B **313**, 155 (1993)
10. H. Komatsu, Prog. Theor. Phys. **67**, 1177 (1982); R. A. Flores, M. Sher, Ann. Phys. (NY) **148** (1983) 295; M. Sher, Phys. Rep. **179** (1989) 273; D. Kominis, R.S. Chivukula, Phys. Lett. B **304**, 152 (1993); S. Nie, M. Sher, Phys. Lett. B **449**, 89 (1999)
11. Y. Grossman, Nucl. Phys. B **426**, 355 (1994)
12. A.K. Grant, Phys. Rev. D **51**, 207 (1995); P.H. Chankowski, M. Krawczyk, J. Zochowski, Eur. Phys. J. C **11**, 661 (1999)
13. CLEO Collaboration, CLEO CONF 98-17, ICHEP98 1011
14. M. Ciuchini, G. Degrassi, P. Gambini, G.F. Giudice, Nucl. Phys. B **527**, 21 (1998); P. Ciafaloni, A. Romanino, A. Strumia, Nucl. Phys. B **524**, 361 (1998); F. Borzumati, G. Greub, Phys. Rev. D **58**, 074004 (1998); **59**, 057501 (1999); T.M. Aliev, E.O. Iltan, Phys. Rev. D **58**, 095014 (1998)
15. J.F. Gunion, H.E. Haber, G. Kane, S. Dawson, The Higgs hunter's guide (Addison-Wesley, New York 1990)
16. S. Alam, K. Hagiwara, S. Kanemura, R. Szalapski, Y. Umeda, Nucl. Phys. B **541**, 50 (1999)
17. A. Djouadi, V. Driesen, W. Hollik, J. Rosiek, Nucl. Phys. B **491**, 68 (1997)
18. A. Dabelstein, Nucl. Phys. B **456**, 25 (1995); M. Böhm, W. Hollik, H. Spiesberger, Fortschr. Phys. **34**, 11 (1986)
19. M. Capdequi Peyranère, Int. Mod. Phys. A **14**, 429 (1999)
20. A.G. Akeroyd, A. Arhrib, M. Capdequi Peyranére, Mod. Phys. Lett. A **14**, 2093 (1999)
21. S. Heinemeyer, W. Hollik, G. Weiglein, J. High Ener. Phys. **0006**, 009 (2000)
22. DELPHI: LEPC talks, Presentations on November 9 1999; (http://delphiwww.cern.ch/˜offline/physics_links/lepc.html)
23. V. Barger, M.S. Berger, P. Ohmann, PRD **47**, 1093 (1993); M. Carena, M. Olechowski, S. Pokorski, C.E.M. Wagner, Nucl. Phys. B **426**, 1994 (269)
24. S.H. Zhu, hep-ph/9901221
25. J.M. Cornwall, D.N. Levin, G. Tiktopoulos, Phys. Rev. Lett. **30**, 1268 (1973); Phys. Rev. D **10**, 1145 (1974); B.W. Lee, C. Quigg, H.B. Thacker, Phys. Rev. D **16**, 1519 (1977)
26. M.S. Chanowitz, M.K. Gaillard, Nucl. Phys. B **261**, 379 (1985); H. Veltman, Phys. Rev. D **41**, 2294 (1990); J. Bagger, C. Schmidt, Phys. Rev. D **41**, 264 (1990); H.-J. He, Y.-P. Kuang, X. Li, Phys. Rev. Lett. **69**, 2619 (1992); Phys. Rev. D **49**, 4842 (1994)

27. K. Odagiri, private communication
28. K. Odagiri, Phys. Lett. B **452**, 327 (1999)
29. A. Arhrib, M. Capdequi Peyranére, W. Hollik, G. Moultaka, hep-ph/9912527
30. G. Passarino, M. Veltman, Nucl. Phys. B **160**, 151 (1979)